Biochimica et Biophysica Acta 1838 (2014) 2662–2669

Contents lists available at ScienceDirect

Biochimica et Biophysica Acta

journal homepage: www.elsevier.com/locate/bbamem

HIV-1 antibodies and vaccine antigen selectively interact with lipid domains

Gregory J. Hardy [a], Gene C Wong [a], Rahul Nayak [a], Kara Anasti [b], Michael Hirtz [c], Joseph G. Shapter [d], S. Munir Alam [b], Stefan Zauscher [a,*]

[a] Mechanical Engineering and Materials Science, Duke University, Durham, NC 27708, United States
[b] Human Vaccine Institute, Duke University School of Medicine, Durham, NC 27708, United States
[c] Institute of Nanotechnology (INT) & Karlsruhe Nano Micro Facility (KNMF), Karlsruhe Institute of Technology (KIT), Eggenstein-Leopoldshafen 76344, Germany
[d] School of Chemical and Physical Sciences, Flinders University, Bedford Park, South Australia 5042, Australia

ARTICLE INFO

Article history:
Received 7 May 2014
Received in revised form 30 June 2014
Accepted 2 July 2014
Available online 11 July 2014

Keywords:
Human immunodeficiency virus-1 (HIV-1)
Supported lipid bilayer
Atomic force microscopy
Lipid domain
Neutralizing antibody

ABSTRACT

The rare, broadly neutralizing antibodies, 4E10 and 2F5, that target the HIV-1 membrane proximal external region also associate with HIV-1 membrane lipids as part of a required first-step in HIV-1 neutralization. HIV-1 virions have high concentration of cholesterol and sphingomyelin, which are able to organize into liquid-ordered domains (*i.e.*, lipid rafts), and could influence the interaction of neutralizing antibodies with epitopes proximal to the membrane. The objective of this research is to understand how these lipid domains contribute to 2F5/4E10 membrane interactions and to antigen presentation in liposomal form of HIV-1 vaccines. To this end we have engineered biomimetic supported lipid bilayers and are able to use atomic force microscopy to visualize membrane domains, antigen clustering, and antibody–membrane interactions. Our results demonstrate that 2F5/4E10 do not interact with highly ordered gel and liquid-ordered domains and exclusively bind to a liquid-disordered lipid phase. This suggests that vaccine liposomes that contain key viral membrane components, such as high cholesterol content, may not be advantageous for 2F5/4E10 vaccine strategies. Rather, vaccine liposomes that primarily contain a liquid-disordered phase may be more likely to elicit production of lipid reactive, 2F5- and 4E10-like antibodies.

1. Introduction

Induction of broadly neutralizing antibodies (NAbs) against HIV-1 remains an exceptional challenge. However, several, rare antibodies have been isolated that are broadly neutralizing, including monoclonal antibodies, 2F5 and 4E10. The neutralizing mechanism of 2F5/4E10 represents a promising framework for the design of new HIV-1 liposomal vaccines. *In-vitro* studies have shown that 2F5/4E10 successfully inhibit the fusion process of HIV-1 by binding the membrane-proximal external region (MPER) of viral gp41 *via* a two-stage mechanism: NAbs 2F5 and 4E10 first interact nonspecifically with the viral lipid membrane and then with the target MPER [1,2]. Induction of polyreactive antibodies that can bind to both, lipids and antigen is thus required for MPER-targeted HIV-1 neutralization. Understanding the role of the lipid membrane in 2F5/4E10's neutralization mechanism can help select important lipid components to be used in the synthesis of vaccine liposomes. We posit that vaccine liposomes that contain the MPER antigen in an lipid environment optimized for 2F5 and 4E10 interactions are more likely to induce the desired, polyreactive NAbs. The research results presented here provide information on lipid selection when developing new immunogen designs against HIV-1.

The interaction between lipids and 2F5/4E10 is likely mediated by the NAb's unique complementary determining region (CDR) H3 loop [3]. The CDR H3 regions contain an unusually large number of hydrophobic and membrane-reactive residues, suggesting that they can embed in the viral membrane and position the NAb to encounter and bind its antigen [4,5]. Mutations in these CDR H3 antibody regions allow 2F5/4E10 to bind MPER's linear and conformational epitopes, but prevent the NAb's lipid reactivity, which results in the inability to bind membrane bound MPER antigen [6]. This phenomenon may explain why simple peptide immunogens that mimic neutralizing epitopes on gp41 do not elicit NAbs *in vivo*, [7] and it is clear that antigen sequence is not the sole determinant of neutralizing ability. To mimic 2F5 and 4E10's *in-vitro* neutralizing ability, *in-vivo* immunogens must elicit antibodies that also react with the HIV-1 lipid envelope. How to design immunogens to do this remains largely unknown.

* Corresponding author at: Department of Mechanical Engineering and Materials Science. 144 Hudson Hall Box 90300 Durham, NC 27708, United States. Tel.: +1 919 660 5360; fax: +1 919 660 8963.
E-mail address: zauscher@duke.edu (S. Zauscher).

http://dx.doi.org/10.1016/j.bbamem.2014.07.007
0005-2736/

1.1. HIV-1 domain formation

It is currently believed that the viral envelope contains highly ordered lipid domains (*i.e.*, lipid rafts) and that these lipid domains influence lipid–NAb interactions. Generally, lipid domains are defined as areas of a membrane that have a different composition from their surroundings, *i.e.*, an enrichment or depletion of certain membrane components. The presence of lipid domains indicates lipid phase separation. There are two main phase types: a solid and a liquid phase. The solid or "gel" phase is characterized by highly ordered, tightly packed lipids that, compared with the liquid phase, have limited lateral mobility (Fig. 1B). The liquid phase can be further divided into the liquid-disordered (L_d) and liquid-ordered (L_o) phases (Fig. 1C). The L_d phase exists when lipids have melted from the gel to liquid phase (defined by the transition temperature, T_m) while the L_o typically forms when cholesterol (CH) and/or sphingomyelin (SM) exist in L_d membranes. CH and SM will co-localize within the L_d phase resulting in highly ordered, tightly packed islands known as L_o domains or lipid rafts [8].

The HIV-1 membrane envelope contains a unique lipid composition that differs from that of host cell membranes [9] because HIV-1 acquires its envelope by budding from isolated islands of membrane lipids enriched in CH and SM [10]. Due to the high concentration of CH and SM in the native HIV-1 envelope, the L_o domain is expected to dominate HIV-1 domain structures. Yet, the size, physical properties, and dynamics of such lipid domains are poorly characterized for the HIV-1 envelope, and it is as of yet unknown how lipid domains contribute to 2F5/4E10-membrane interactions and MPER antigen presentation.

1.2. Supported lipid bilayer model membrane platform

To help understand how lipid domains influence NAb- and antigen-membrane interactions we have created supported lipid bilayers (SLBs) that can phase separate spontaneously into stable lipid domain structures (Fig. 1). Because SLBs can recapitulate the lateral lipid diffusivity of native cell membranes and are stable and confined in two dimensions to the substrate surface, they can be used to model the composition, organization, and properties of native lipid bilayers [11].

Although several spectroscopy-based techniques have been used to help understand the role of lipids in 2F5/4E10 HIV-1 neutralization and vaccine design, [12,13] these techniques lack high lateral resolution and cannot visualize how membrane morphology, such as lipid domains, contribute to NAb- and antigen-membrane interactions. To visualize NAb- and antigen-membrane interactions, we used atomic force microscopy (AFM) [14] to produce high-resolution, topographical images of three different SLBs: an L_d SLB, an L_d–gel SLB, and an L_d–L_o SLB made from a complex, five-component lipid mixture that mimics the lipid composition of the native HIV-1 envelope.

Unlike many surface-sensitive, spectroscopy techniques, AFM can visualize how antibodies and antigens spatially interact with lipid domains. We show that AFM reveals the height mismatch between lipid domains and surface-associated proteins with Ångstrom vertical resolution and approximately 5–10 nm lateral resolution. By visualizing these interactions, we provide important information for the design of vaccine liposomes that optimize membrane-dependent antibody binding and antigen presentation.

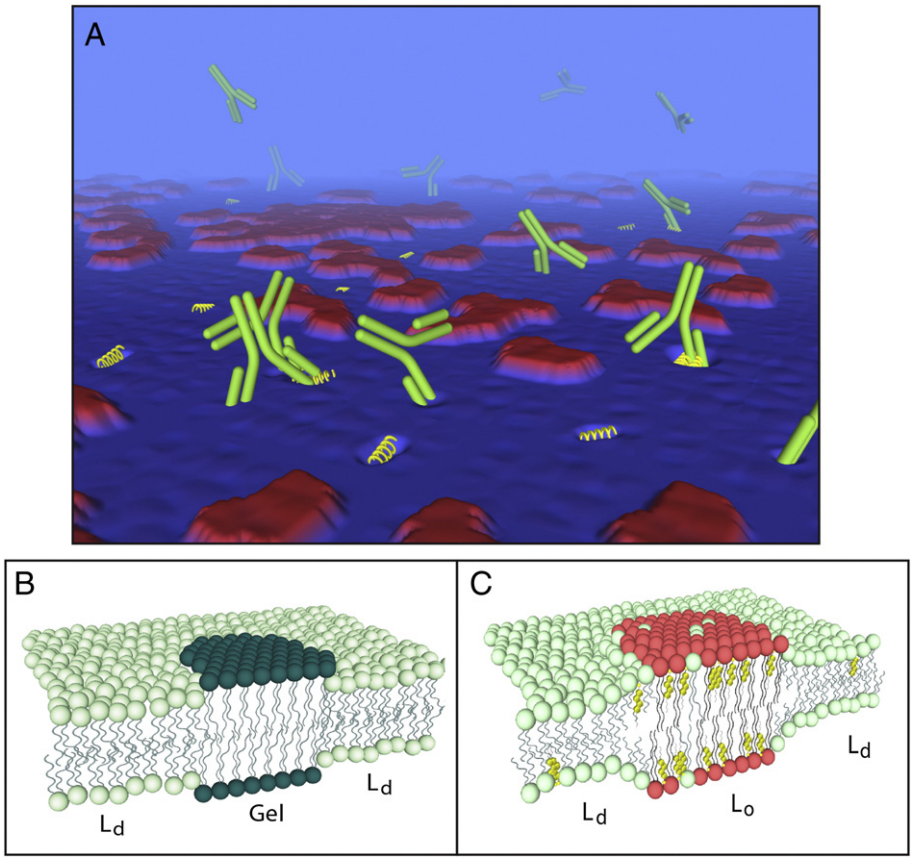

Fig. 1. Schematic representation of NAbs, antigen, and lipid organization in SLBs. (A) Proposed SLB environment interacting with NAbs (green) and $MPER_{656}$ (yellow). NAbs and $MPER_{656}$ only interact with the L_d phase (blue) and avoid L_o and gel domains (represented collectively in red). (B) Lipid organization expected from the POPC:POPE SLB. Gel domain (dark green) surrounded by L_d phase (light green). (C) Lipid organization expected from the model HIV SLB. L_o domains consisting of sphingomyelin (red) and cholesterol (yellow) in a L_d phase (light green).

2. Results

2.1. Antibody and antigen interactions with L_d SLBs

AFM height images of 1-palmitoyl-2-oleoyl-sn-glycero-3-phosphocholine (POPC) SLBs are shown in Figs. 2A–D. In these, and all following AFM height images, increasing topographical feature heights are represented by increasing brightness. The POPC SLB appears smooth, with no observable height differences in the membrane organization (Fig. 2A). This smooth topography reflects the presence of a homogenous lipid phase with no observable domain formation. Since the T_m of POPC is −2 °C, the SLB exists in the L_d phase at room temperature.

2F5 and 4E10 were each separately added to the POPC SLBs. After NAb addition, the AFM height images (Figs. 2B,C) reveal bright spots (*i.e.*, topographical peaks) over the entire membrane surface; we attribute these peaks to the presence of NAbs that have interacted with the top leaflet of the SLB. The surface-associated NAbs cover approximately 3% of the SLB surface (Table 1). Based on topographical feature size distributions, the surface-associated NAbs are distributed between 0.5–1.5 nm above the SLB with few feature counts at 2 nm and greater. Features exceeding 2 nm in height likely reflect clusters of antibodies bound to the SLB. In solution, antibodies such as 2F5 and 4E10 have a radius of gyration of approximately 7 nm [15]. The small heights of the topographic peaks suggest that in most instances individual antibodies are bound to the SLB surface. We attribute the apparent size difference (*i.e.*, height of NAbs on the SLB surface *vs.* Ab size in solution) to the tapping force exerted by the AFM cantilever during imaging. This force compresses the antibody against and possibly into the SLB, which results in the smaller observed heights.

Table 1
Average percent surface coverage (± standard error of the mean) NAb binding for all SLBs tested (calculated from AFM topographical images). (–) Indicates NAb coverage was undetermined.

SLB	2F5 coverage (%, n = 3)		4E10 coverage (%, n = 3)	
	L_d area	Total area	L_d area	Total area
POPC	3 ± 0	3 ± 0	3 ± 0	3 ± 0
POPC:MPER	42 ± 6	42 ± 6	47 ± 5	47 ± 5
POPC:POPE	3 ± 1	1 ± 0	3 ± 0	1 ± 0
POPC:POPE:MPER	26 ± 7	10 ± 3	19 ± 2	8 ± 1
Model HIV	–	4 ± 1	–	2 ± 0
Model HIV:MPER	–	2 ± 1	–	2 ± 0

$MPER_{656}$ consists of an amphipathic GTH1 membrane anchor tag and the binding epitope for both 2F5 and 4E10 [16]. While the GTH1 anchor resides within the hydrophobic core of the SLB, the NAb binding epitopes are likely positioned parallel with the top lipid leaflet, *i.e.*, at the interface of the lipid bilayer and bulk solution [17]. Based on the size of the MPER binding epitope (3.3 kDa), the folded length is approximately 2 nm. When $MPER_{656}$ is included in the POPC SLB (Fig. 2E), 0.5 nm high topographical peaks appear evenly distributed over the SLB surface. This subtle, antigen-induced height difference between the POPC and POPC:$MPER_{656}$ SLB is further confirmed by the root mean squared (RMS) surface roughness. Over a 1 μm^2 area, the RMS roughness of the POPC:$MPER_{656}$ SLB is 2.7 ± 0.2 Å, while that of the neat POPC bilayer is significantly smaller, with 1.6 ± 0.05 Å. This

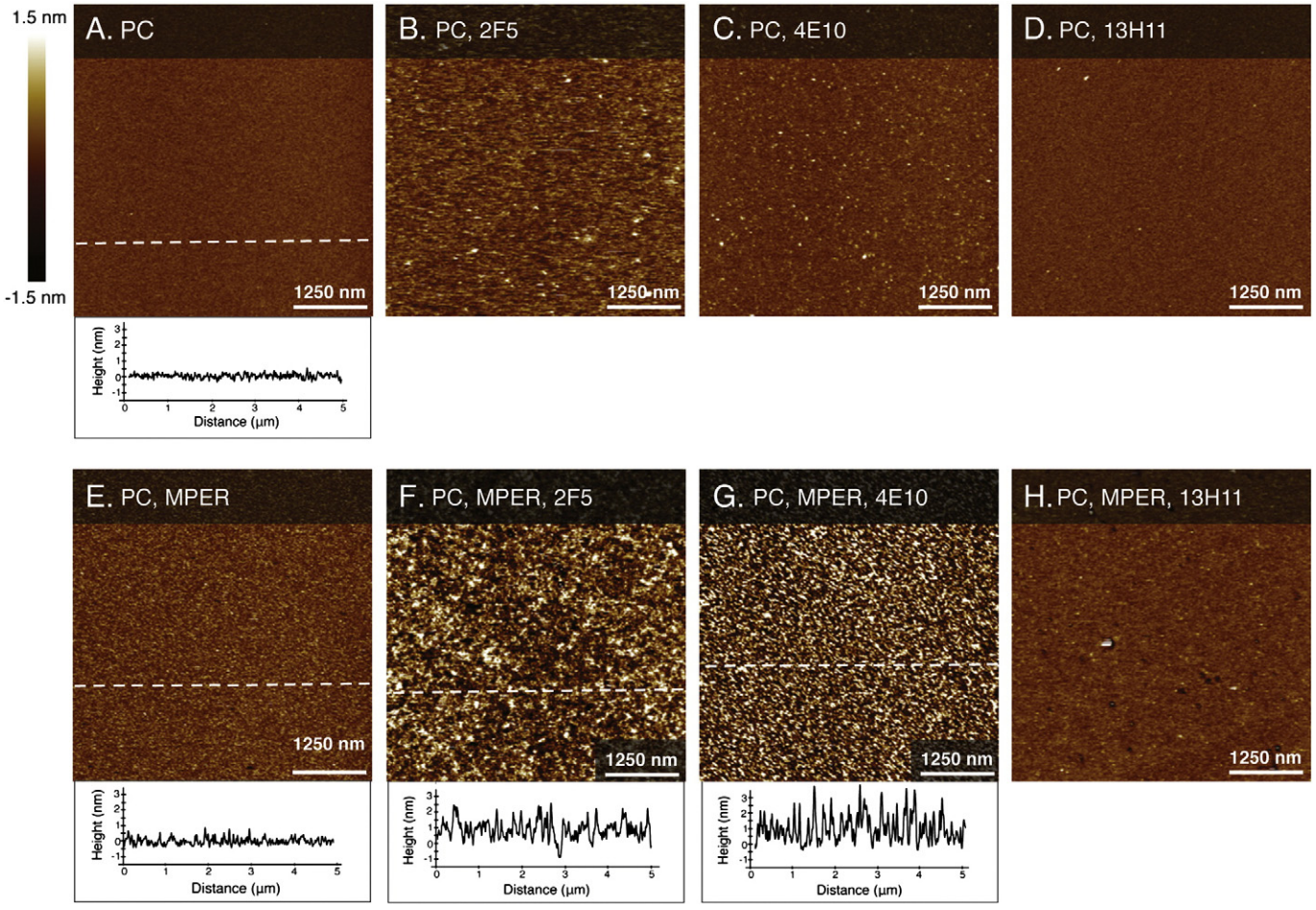

Fig. 2. AFM height images of the POPC and POPC:$MPER_{656}$ SLBs with and without antibody addition (imaged in liquid at 24 °C). Height cross-section given for select images. (A) POPC SLB. (B–D) 2F5, 4E10 and 13H11 added to the POPC SLB, respectively. (E) POPC:$MPER_{656}$ SLB. (F–H) 2F5, 4E10, and 13H11 added to the POPC:$MPER_{656}$ SLB, respectively.

difference in SLB surface roughness can also be seen by comparing the height cross-sections from Fig. 2A and E, presented below the topography images.

When NAbs are incubated on these SLB surfaces, they bind preferentially to regions that contain $MPER_{656}$ antigen (Fig. 2F,G). NAb binding to the SLB and to $MPER_{656}$ can be seen by the appearance of "bright spots", *i.e.*, peaks 2–4 nm in height, in the SLB height images. The locations of these peaks are evenly distributed across the SLB surface, suggesting that $MPER_{656}$ is also evenly distributed. 2F5's surface coverage is 42 ± 6%, while addition of 4E10 results in a surface coverage of 47 ± 5% (Table 1).

A murine monoclonal antibody, 13H11, was incubated on all SLB surfaces as control. 13H11 has no lipid reactivity and while it does bind to the soluble form of the MPER-antigen peptide, it cannot bind to membrane-embedded MPER [2]. As expected, there is little to no 13H11 interactions with the POPC SLB (Fig. 2D) nor with POPC SLB containing MPER (Fig. 2H), thus confirming that NAb-membrane interactions are specific to 2F5 and 4E10.

2.2. Antibody and antigen interactions with L_d–Gel SLBs

While NAbs and $MPER_{656}$ are apparently evenly distributed throughout the L_d phase of the unary POPC SLB, we next tested their distribution in a binary, phase-separated SLB, consisting of POPC:1-palmitoyl-2-oleoyl-sn-glycero-3-phosphoethanolamine (POPE) (1:1). POPC:POPE SLBs, imaged at 18–20 °C (Fig. 3A), revealed a gel domain consisting of predominantly POPE (T_m = 25 °C) and an L_d phase consisting of predominantly POPC (T_m = −2 °C). Gel domains are taller and appear brighter compared to the L_d phase, which is lower and thus appears darker. The taller POPE gel domains extend 4.8 ± 0.4 Å above the surrounding POPC L_d phase. When NAbs were incubated on this phase-separated SLB surface, they interacted only with the L_d phase (Fig. 3B,C), resulting in a surface coverage on the L_d phase of 3 ± 1% for 2F5 and 3 ± 0% for 4E10, respectively (Table 1). The tallest NAb peaks were approximately 1.5 nm above the L_d domain surface.

Next, POPC:POPE:$MPER_{656}$ SLBs were prepared. AFM images (Fig. 3E) revealed that $MPER_{656}$ exclusively localized to the L_d domain.

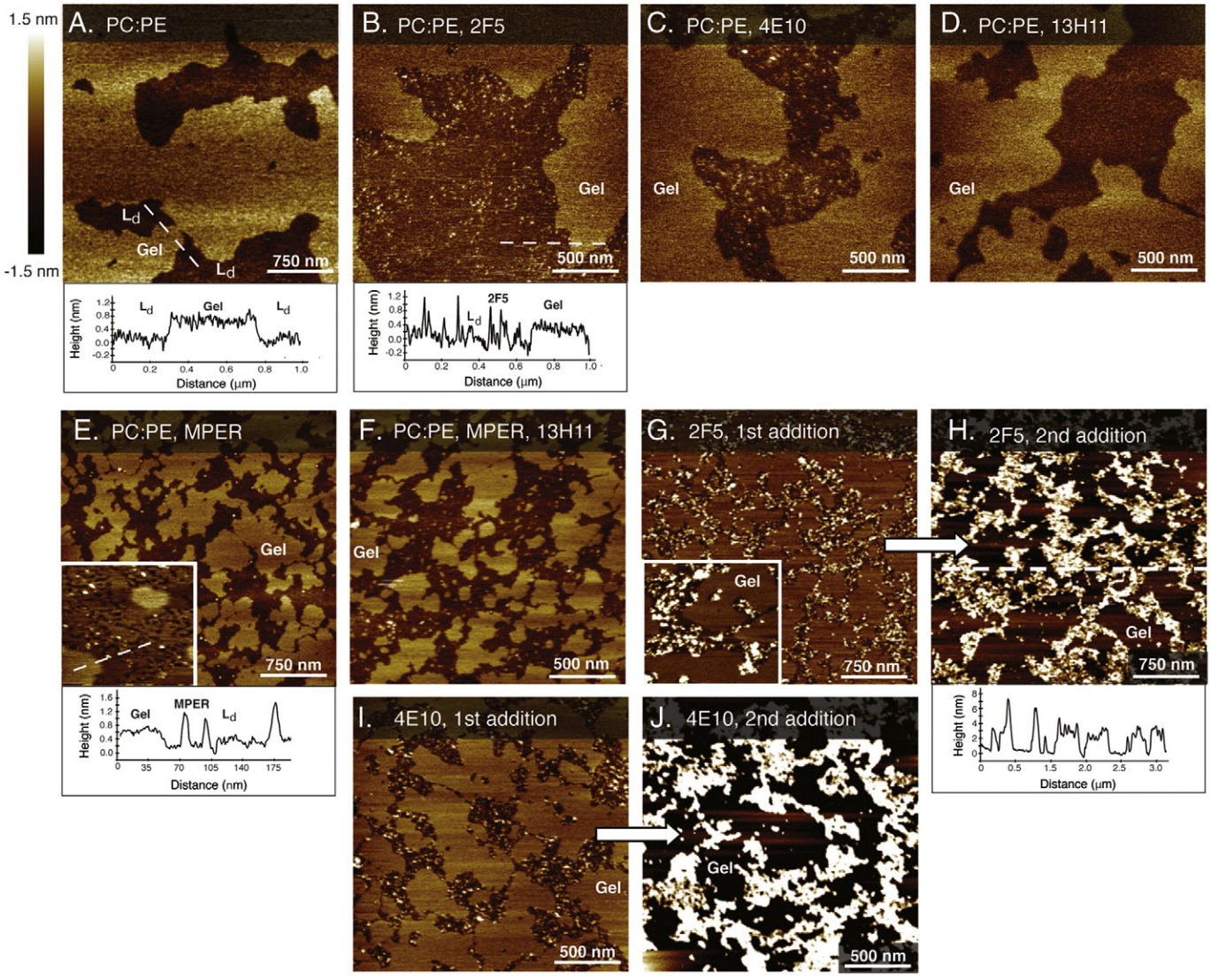

Fig. 3. AFM height images of the POPC:POPE and POPC:POPE:$MPER_{656}$ SLBs with and without antibody addition (imaged in liquid at 18–20 °C). Height cross-section given for select images. (A) POPC:POPE SLB. The bright area is the taller, gel domain, while the darker area is the lower, L_d phase. (B–D) 2F5, 4E10, and 13H11 added to the POPC:POPE SLB, respectively. (E) POPC:POPE:$MPER_{656}$ SLB. Inset: 250 × 250 nm height image from a replicate sample showing $MPER_{656}$ in the L_d phase. (F) 2F5 added to the POPC:POPE:$MPER_{656}$ SLB. Inset: 250 × 250 nm image from a replicate sample (G) image (F) with a second addition of 2F5 (4.0 μM). (H,I) Repeated conditions from images (F,G) with 4E10. (M) 13H11 added to POPC:POPE:$MPER_{656}$ SLB.

While the antigen peak heights ranged from about 0.5 nm to 2.0 nm, the peak widths ranged from about 15 to 30 nm, *i.e.*, much wider than expected for single $MPER_{656}$ peptides. This observation suggests that $MPER_{656}$ aggregated in the L_d phase.

When NAbs were added to the POPC:POPE:$MPER_{656}$ SLB, they bound to the SLB and to $MPER_{656}$, indicated by the presence of 1–2 nm peaks in the AFM images (Fig. 3G,I). These images also show that NAbs only bound to the L_d phase and were excluded from the taller, gel phase. 2F5's L_d surface coverage was 26 ± 1%, while 4E10 addition resulted in an L_d surface coverage of 19 ± 2% (Table 1). A second addition of NAbs (4.0 μM) resulted in large clusters (3–7 nm tall) of L_d-localized NAb (Fig. 3H,J) reaching close to 100% coverage of the L_d phase. No antibody binding peaks were found in the gel domains, which suggest that gel domains are either void of $MPER_{656}$, or the antigen is presented in a conformation that is not accessible to NAb binding.

As expected, 13H11 showed no interactions with either the POPC:POPE (Fig. 3D) or the POPC:POPE:$MPER_{656}$ SLB (Fig. 3F).

2.3. Antibody and antigen interactions with model HIV-1 SLBs

A common SLB model of the HIV-1 envelope is a ternary composition consisting of POPC, SM, and CH [18,19]. Here we use a more physiologically relevant SLB model of the HIV-1 envelope [20] to study NAb and antigen interactions. Our model HIV SLB composition consists of POPC, POPE, 1-palmitoyl-2-oleoyl-sn-glycero-3-phospho-L-serine (POPS), brain SM, and CH in a molar ratio of 9.35:19.25:8.25:18.15:45.00. This composition was previously used to make liposomes for SPR binding assays in vaccine studies [6,21]. To create SLBs with this model HIV composition, we have previously developed a vesicle fusion technique that uses amphipathic, α-helical (AH) peptides as a catalyst to generate complex SLBs with high cholesterol content [22]. Here, for the first time, we imaged with AFM to visualize NAb and antigen interactions with this model HIV SLB.

Fig. 4 demonstrates the significant morphological changes that occur in the model HIV SLB when imaged at 18 °C compared to 37 °C. At 18 °C

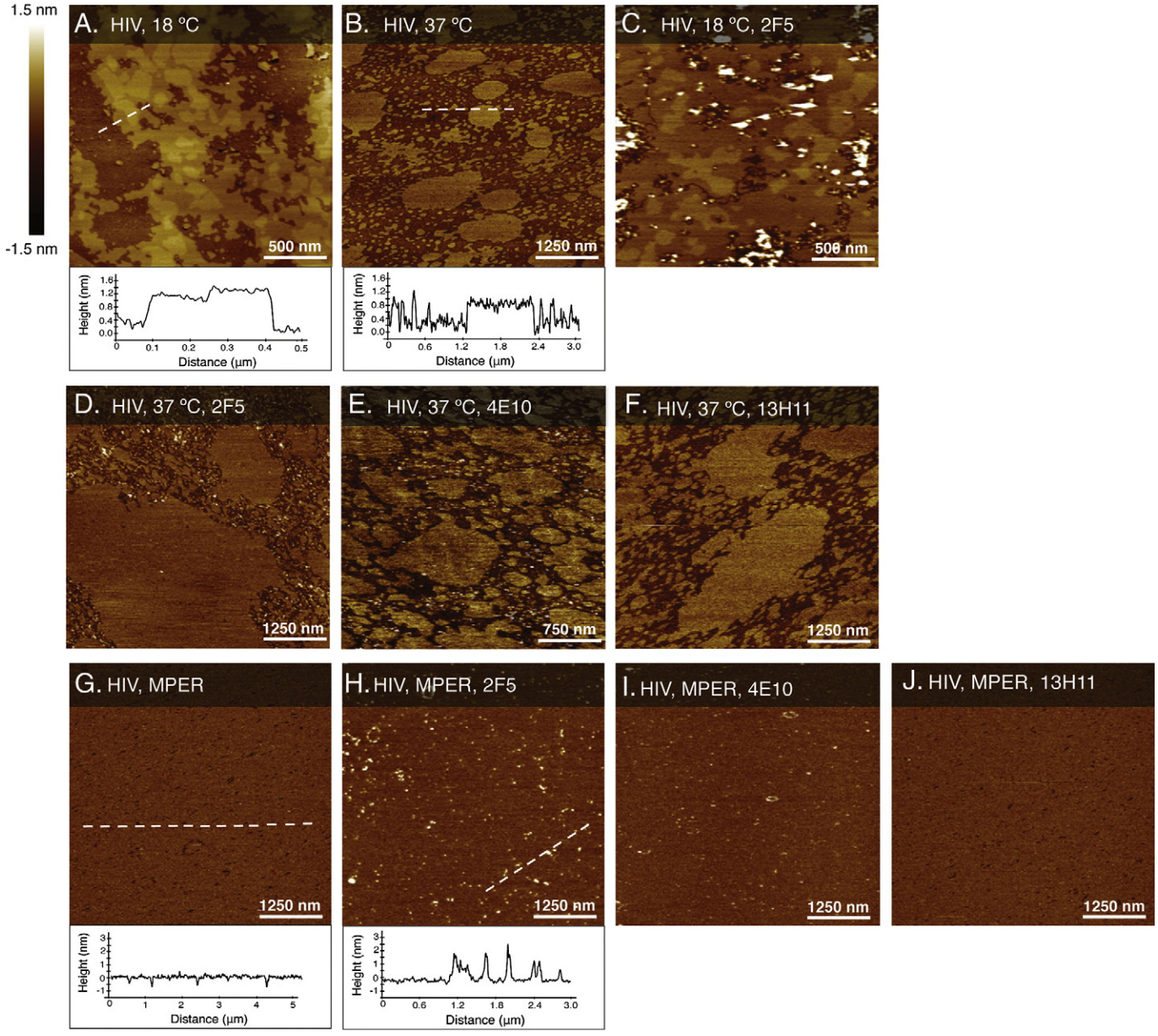

Fig. 4. AFM height images of the model HIV and model HIV:$MPER_{656}$ SLB with and without antibody addition. Height cross-section of SLBs given below select images. (A,B) Model HIV SLB imaged at 18 °C and 37 °C, respectively. (C,D) 2F5 added to the model HIV SLB at 18 °C and 37 °C, respectively. (E,H) 4E10 and 13H11 added to the model HIV SLB at 37 °C, respectively (G) Model HIV:$MPER_{656}$ SLB at 37 °C. (H–J) 2F5, 4E10, and 13H11 added to the model HIV SLB:$MPER_{656}$, respectively (at 37 °C).

there are three distinct domains visible (Fig. 4A) with a height difference of 10.3 ± 0.6 Å between the lowest and medium height domains, and a height difference of 2.4 ± 0.7 Å between the medium height and tallest domains. At 37 °C (Fig. 4B), however, only two distinct phases exist, with a height difference of 8.2 ± 0.4 Å.

Regardless of temperature, the addition of 2F5 resulted in 2F5-membrane interactions only in the most disordered (*i.e.*, lowest height) lipid phase (Fig. 4C,D). To mimic physiological conditions, comprehensive measurements were conducted on model HIV SLBs at 37 °C. We found that 2F5 had a surface coverage of 4 ± 1%, and that 4E10 behaved like 2F5, by binding only to the most disordered lipid phase (Fig. 4E), reaching a surface coverage of 2 ± 0% (Table 1).

When $MPER_{656}$ was incorporated in the model HIV SLB (37 °C), the prominent, two-phase SLB no longer existed (Fig. 4G–J). Rather, a more homogenous lipid phase, with small, about 7 Å deep, narrow depressions appeared in the bilayer (Fig. 4G). We surmise that these depressions consist largely of the L_d phase, likely containing also $MPER_{656}$. The surface coverage of these L_d features is 3 ± 0%, *i.e.*, significantly less than the surface coverage of the L_d area on the model HIV SLB without antigen (39 ± 3%). Upon addition of NAb, the antibodies only bound to these depressions (Fig. 4H,I), resulting in a NAb total surface coverage of 2 ± 1% and 2 ± 0% for 2F5 and 4E10, respectively (Table 1). The taller, homogenous lipid phase is void of any antigen or antibody binding. Addition of 13H11 resulted in little to no interactions with the HIV SLB in absence (Fig. 4F) and presence (Fig. 4J) of $MPER_{656}$.

Surface plasmon resonance (SPR) experiments (Fig. S1) revealed that NAb binding was significantly higher on the POPC:$MPER_{656}$ membrane compared with binding on the model HIV:$MPER_{656}$ membrane (Figs. S1A,B *vs.* S1D,E). The R_{max} (maximum binding capacity) for POPC:$MPER_{656}$ was 65 ± 9 and 214 ± 10 response units (RU) for 4E10 and 2F5, respectively. For the model HIV:$MPER_{656}$ membrane, the R_{max} dropped to 9 ± 2 RU for 4E10 while binding of 2F5 was even weaker, and no reliable R_{max} values could be determined. These results qualitatively agree with our surface coverage (*i.e.*, binding) measurements by AFM imaging, which showed NAb coverage to be between 42 and 47% for the POPC:$MPER_{656}$ SLB compared to only 2 to 4% for the model HIV:$MPER_{656}$ SLB. For the POPC and the model HIV membrane, 4E10 resulted in an R_{max} of 7 ± 2 and 5 ± 0 RU, respectively, while 2F5 resulted in an undetectable R_{max}. SPR measurements showed no detectable interactions of 13H11 for all membrane compositions tested (Fig. S1C,F).

3. Discussion

3.1. NAb interactions with SLBs

AFM imaging of NAbs interacting with the POPC and POPC:POPE SLB revealed that 2F5 and 4E10 exclusively interacted with the L_d membrane phase. For the POPC SLB the L_d phase made up 100% of the SLB area, while for the POPC:POPE SLB, the L_d area was 41 ± 4%. Despite the difference in L_d area, NAb binding coverage was about 3% on both SLBs. NAb coverage on the L_d area for the model HIV SLB could not be determined accurately due to the dispersed nature and small size of the L_d phase. Instead, we report NAb coverage relative to the total area of the model HIV SLB (Table 1). NAb binding on the model HIV SLB was similar to that on the POPC and POPC:POPE SLBs. NAbs exclusively interacted with the lipid phase with the lowest height and therefore the lowest lipid packing density, the largest membrane disorder, and the highest lipid diffusivity [23–25]. This result is in agreement with a previous AFM study completed by Franquelim et al. [18]. The lipid diffusivity in the L_o phase is approximately a factor 2–10 smaller than in the L_d phase, depending on experimental details [26–28]. The presence of cholesterol is a major contributor to the physical properties of lipid domains. It has been shown that the force required to break the intermolecular lipid interactions in a cholesterol-rich L_o phase is greater compared to that in a cholesterol-depleted L_d phase [25]. This supports the hypothesis that the high order of L_o and gel domains prevented NAb insertion into these SLB areas.

Given the overall compositional and structural complexity of the model HIV SLB, the detailed lipid compositions of individual domains are unclear, but can be estimated considering the T_m values of the lipids. At 18 °C, the domain with the lowest height likely contains the highest concentration of POPC ($T_m = -2$ °C) and POPS ($T_m = 14$ °C). The middle and tallest domains likely contain the highest concentration of POPE ($T_m = 25$ °C), SM ($T_m = 37$ °C), and CH. When the temperature is increased from 18 °C to 37 °C, the SLB transitions from three to two phases. This two-phase system is likely a result of CH and SM redistributing to form discrete L_o–L_d domains. At 37 °C, an L_o–L_d forming bilayer of the model HIV SLB agrees with the phase diagram of a similar bilayer composition, *i.e.*, POPC:PSM:CH (1:1:1) [29]. X-ray diffraction experiments of another, similar bilayer composition, *i.e.*, DOPC:SM:CH (1:1:1), confirm the absence of a gel phase. This suggests that our model SLB also lacks a gel phase, and thus contains a L_d and L_o phase instead [30]. Furthermore, at 37 °C, our model HIV domain height difference is 8.2 ± 0.4 Å, which agrees with expected L_o–L_d height differences. For example, Rinia et al. report similar height differences observed by AFM for DOPC:SM:CH bilayers that phase separate into L_o–L_d domains [31]. Thus, we believe that a L_d phase exists in our model HIV SLB, and that since the L_d phase contains the highest lipid disorder, it should reside in the domains of lowest SLB height, *i.e.*, the same domains to which NAbs bind. This suggests that NAbs interact exclusively with the L_d phase in the model HIV SLB.

Collectively, our experiments on the three SLB systems tested, demonstrate that NAbs 2F5/4E10 bind exclusively to the L_d phase and do not interact with the ordered gel and L_o domains. This also suggests that these NAbs likely target L_d regions on the native virus before binding to their MPER antigen on gp41. To elicit antibodies that can recognize and interact with the L_d phase, vaccine liposomes likely should also contain lipids that organize into a dominant L_d phase. However, as discussed below, vaccine antigens may adversely contribute to L_d formation.

3.2. Antigen and NAb interactions with SLBs

On the POPC SLB (L_d), antigen presentation and NAb binding was uniformly distributed across the entire SLB surface. This indicates that the L_d phase does not restrict or hinder antibody/antigen membrane interactions and facilitates high antibody to antigen binding. In the POPC:POPE:$MPER_{656}$ SLB (gel-L_d), $MPER_{656}$ resided exclusively in the L_d phase. Gel domains not only excluded NAb interactions, but also prevented $MPER_{656}$ membrane integration. The presence of $MPER_{656}$ also inhibited gel domain coalescence. This is seen in Fig. 3 where, in presence of antigen, smaller gel domains still exist (Fig. 3E) when compared to the gel domains in absence of antigen (Fig. 3A). However, the overall L_d area remains relatively constant, *i.e.*, 41 ± 4% without and 39 ± 2% with $MPER_{656}$. The presence of $MPER_{656}$ in the model HIV SLB, decreased the total L_d area substantially. Without $MPER_{656}$, the model HIV SLB had an L_d coverage of 39 ± 3%, and with $MPER_{656}$ the L_d area decreased to 3 ± 0%. When comparing the morphology between the model HIV SLB without and with $MPER_{656}$ (Fig. 4B *vs.* 4G), the presence of antigen resulted in a more homogenous lipid phase that is void of antigen–NAb binding. Large L_d areas fail to form, and the antigen is likely limited to the location of small (~30–60 nm in diameter) L_d pockets. This antigen distribution is in stark contrast to that in the POPC:$MPER_{656}$ (Fig. 2E) and POPC:POPE:$MPER_{656}$ (Fig. 3E) SLBs, where antigen is evenly distributed across the entire L_d phase. The NAb binding coverage is the lowest in the model HIV:$MPER_{656}$ SLB (2 ± 0% for both 2F5 and 4E10) compared to that on POPC:$MPER_{656}$ and POPC:POPE:$MPER_{656}$ SLBs.

SPR experiments confirmed that there is substantially less NAb–$MPER_{656}$ binding when $MPER_{656}$ is included in the highly ordered model HIV SLB when compared to the more fluid POPC SLB. Since

both SLBs were prepared with an equal amount of $MPER_{656}$, we believe that the reduced NAb binding to the model HIV:$MPER_{656}$ SLB arises from the membrane structure and the organization of $MPER_{656}$ in the SLB. AFM topography images suggest that an ordered phase dominates in the model HIV membrane (~97% surface coverage). Either this ordered phase is completely void of $MPER_{656}$ or the antigen is buried in such an orientation that it cannot be detected by NAbs (or by the AFM cantilever during imaging). AFM images also show that $MPER_{656}$ appears to be restricted to the small pockets in the SLB that contain the L_d phase (~3% surface coverage). Only a limited number of NAbs can bind $MPER_{656}$ in these areas (Fig. 4H,I), before steric restrictions likely prevent unbound NAbs from accessing unbound antigens, thus severely limiting NAb–antigen interactions.

4. Conclusions

Our results on SLBs demonstrate that NAbs 2F5/4E10 do not interact with the highly ordered gel or L_o phase but exclusively bind to the L_d phase. Using vaccine liposomes that mimic the high order of the HIV-1 envelope to induce antibodies that can recognize and bind to the viral envelope, may, thus not be advantageous for 2F5/4E10 based vaccine strategies. Rather, vaccine liposomes that contain an L_d phase may provide optimal selection of 2F5- and 4E10-like antibodies.

In the context of liposomal antigen presentation, our results suggest that the presence of the $MPER_{656}$ peptide may severely limit the L_d area available for antibody interactions. Subsequently, this reduces the amount of $MPER_{656}$ that is accessible for 2F5/4E10 binding, since $MPER_{656}$ preferentially localizes to the L_d area. If L_d forming lipid components are used in vaccine liposomes, it is important to ensure that the presence of antigen does not inhibit large-scale L_d formation.

5. Materials and methods

5.1. Antibodies and antigen

Anti-HIV-1 gp41 (anti-membrane proximal) NAbs 4E10 and 2F5 were purchased from Polymun, Inc., Vienna, Austria. Mouse mAb 13H11 was produced from splenocytes from a mouse immunized with HIV Env oligomer CON-S [32], as described.[33] SLBs containing embedded HIV antigen, $MPER_{656}$-GTH1 (CPC Scientific Inc., San Jose, CA) were prepared by first dissolving antigen in chloroform and then adding to lipid mixture before being dried under nitrogen.

5.2. Lipid preparation

POPC, POPE, POPS, SM, and CH in chloroform (Avanti Polar Lipids, Alabaster, Al) was brought to room temperature, dried under nitrogen, and then dried under vacuum for three hours. The lipid film was reconstituted in 37 °C PBS without Ca^{2+} and Mg^{2+}, pH 7.4 (Gibco Invitrogen, Grand Island, NY), vortexed, sonicated, and extruded 11 times through a 0.4 μm filter (Whatman, Florham Park, NJ), and then through a 0.1 μm filter [34]. The concentrated lipid solution was then diluted to 0.4 mg/mL in PBS buffer and vortexed immediately before use. After lipid extrusion, vesicle solutions were used within eight hours.

5.3. AFM imaging

The AFM images presented are the highest quality images that are representative of the observations obtained from image replicates ($n = 3$ for SLBs containing antibodies and $n \geq 4$ for all other SLBs). Unless otherwise noted, NAbs were added at approximately 4.7 μM for SLBs without $MPER_{656}$ and 2.0 μM for SLBs with $MPER_{656}$. Control antibody, 13H11 was added at 4.7 μM for all membranes tested. AFM imaging was performed using a commercial AFM (Nanoscope IV, Digital Instruments/Bruker, Santa Barbara, CA) operating at room temperature. Images were obtained in buffer with tapping mode using triangular Si_3N_4 cantilevers (Bruker, SNL-10) with a spring constant of 0.06 N m^{-1}. The formation of SLBs for AFM imaging was achieved by α-helical (AH) peptide-induced vesicle fusion as previously described. [22] Antibodies were added to SLB samples between AFM scans by pipetting 20–50 μL of buffer containing antibodies to the water meniscus on the mica sample. For experiments at 37 °C, a Thermal Applications Controller (Bruker, Santa Barbara, CA) was used to heat the sample. Percent coverage of lipid domains and bound antibodies to SLB surfaces was calculated using height images analyzed with ImageJ software. SLB RMS values ($n = 4$) were calculated with NanoScope Analysis software.

5.4. Surface plasmon resonance

Surface plasmon resonance (SPR) measurements were performed on a BIAcore 3000 (BIAcore Inc., Uppsala, Sweden) instrument. Antibody binding (100 ug/mL) was monitored in real-time at 25 °C with a continuous flow of PBS, pH 7.4 (Gibco Invitrogen, Grand Island, NY) at 20 μL/min for 2 min. For lipid surfaces, approximately 500 RU of liposomes were captured on a BIAcore SPR L1 chip. BIAevaluation 3.0 software (BIAcore Inc.) was used to determine R_{max} values. A bivalent analyte model was used to fit the binding curves of 2F5/4E10-POPC:MPER interactions and a Langmuir 1:1 model was used to fit the binding curves of all other antibody-membrane interactions.

Supplementary data to this article can be found online at http://dx.doi.org/10.1016/j.bbamem.2014.07.007.

Acknowledgements

G.J.H. and S.Z. gratefully acknowledge the financial and training support from the Center for Biomolecular and Tissue Engineering (Duke University), the Structural Biology and Biophysics program (Duke University), and the Karlsruhe House of Young Scientists (Karlsruhe Institute of Technology). This research was supported by the NIH/NIAID, grant AI102814-01 (S.Z. and S.M.A.), by the East Asia and Pacific Summer Institutes program, grant NSF 1108266 (G.J.H.), and by the Australian Microscopy and Microanalysis Research Facility (AMMRF) (J.G.S.).

References

[1] G.R. Matyas, et al., Neutralizing antibodies induced by liposomal HIV-1 glycoprotein 41 peptide simultaneously bind to both the 2F5 or 4E10 epitope and lipid epitopes, AIDS 23 (16) (2009) 2069–2077.
[2] S.M. Alam, et al., The role of antibody polyspecificity and lipid reactivity in binding of broadly neutralizing anti-HIV-1 envelope human monoclonal antibodies 2F5 and 4E10 to glycoprotein 41 membrane proximal envelope epitopes, J. Immunol. 178 (7) (2007) 4424–4435.
[3] G. Ofek, et al., Structure and mechanistic analysis of the anti-human immunodeficiency virus type 1 antibody 2F5 in complex with its gp41 epitope, J. Virol. 78 (19) (2004) 10724–10737.
[4] G. Ofek, M. Tang, A. Sambor, H. Katinger, J.R. Mascola, R. Wyatt, P.D. Kwong, Structure and mechanistic analysis of the anti-human immunodeficiency virus type 1 antibody 2F5 in complex with its gp41 epitope, J. Virol. 78 (19) (2004) 10724–10737.
[5] R.M.F. Cardoso, et al., Broadly neutralizing anti-HIV antibody 4E10 recognizes a helical conformation of a highly conserved fusion-associated motif in gp41, Immunity 22 (2) (2005) 163–173.
[6] S.M. Alam, et al., Role of HIV membrane in neutralization by two broadly neutralizing antibodies, Proc. Natl. Acad. Sci. U. S. A. 106 (48) (2009) 20234–20239.
[7] S.M. Dennison, et al., Induction of antibodies in rhesus macaques that recognize a fusion-intermediate conformation of HIV-1 gp41, PLoS ONE 6 (11) (2011).
[8] K. Simons, E. Ikonen, Functional rafts in cell membranes, Nature 387 (6633) (1997) 569–572.
[9] B. Brugger, et al., The HIV lipidome: a raft with an unusual composition, Proc. Natl. Acad. Sci. U. S. A. 103 (8) (2006) 2641–2646.
[10] R.C. Aloia, H. Tian, F.C. Jensen, Lipid composition and fluidity of the human immunodeficiency virus envelope and host cell plasma membranes, Proc. Natl. Acad. Sci. U. S. A. 90 (11) (1993) 5181–5185.
[11] L.C. Kam, Capturing the nanoscale complexity of cellular membranes in supported lipid bilayers, J. Struct. Biol. 168 (1) (2009) 3–10.
[12] P.N. Reardon, et al., Structure of an HIV-1-neutralizing antibody target, the lipid-bound gp41 envelope membrane proximal region trimer, Proc. Natl. Acad. Sci. U. S. A. 111 (4) (2014) 1391–1396.

[13] G.J. Hardy, et al., Screening the interactions between HIV-1 neutralizing antibodies and model lipid surfaces, J. Immunol. Methods 376 (1–2) (2012) 13–19.
[14] S. Morandat, S. Azouzi, E. Beauvais, A. Mastouri, K. El Kirat, Atomic force microscopy of model lipid membranes, Anal. Bioanal. Chem. 405 (5) (2013) 1445–1461.
[15] L. Cser, I.A. Gladkih, F. Franek, Y.M. Ostanevich, Investigation of antibody structures by scattering techniques, Colloid Polym. Sci. 259 (6) (1981) 625–640.
[16] S.M. Dennison, et al., Stable docking of neutralizing human immunodeficiency virus type 1 gp41 membrane-proximal external region monoclonal antibodies 2F5 and 4E10 is dependent on the membrane immersion depth of their epitope regions, J. Virol. 83 (19) (2009) 10211–10223.
[17] Z.Y.J. Sun, et al., HIV-1 broadly neutralizing antibody extracts its epitope from a kinked gp41 ectodomain region on the viral membrane, Immunity 28 (1) (2008) 52–63.
[18] H.G. Franquelim, et al., Anti-HIV-1 antibodies 2F5 and 4E10 interact differently with lipids to bind their epitopes, AIDS 25 (4) (2011) 419–428.
[19] A. Saez-Cirion, et al., Sphingomyelin and cholesterol promote HIV-1 gp41 pretransmembrane sequence surface aggregation and membrane restructuring, J. Biol. Chem. 277 (24) (2002) 21776–21785.
[20] B. Brugger, et al., The HIV lipidome: a raft with an unusual composition, Proc. Natl. Acad. Sci. U. S. A. 103 (8) (2006) 2641–2646.
[21] H. Mouquet, et al., Polyreactivity increases the apparent affinity of anti-HIV antibodies by heteroligation, Nature 467 (7315) (2010) (591-U117).
[22] G.J. Hardy, et al., Biomimetic supported lipid bilayers with high cholesterol content formed by alpha-helical peptide-induced vesicle fusion, J. Mater. Chem. 22 (37) (2012) 19506–19513.
[23] A. Mecke, D.K. Lee, A. Ramamoorthy, B.G. Orr, M.M.B. Holl, Membrane thinning due to antimicrobial peptide binding: an atomic force microscopy study of MSI-78 in lipid bilayers, Biophys. J. 89 (6) (2005) 4043–4050.
[24] G. M'Baye, Y. Mely, G. Duportail, A.S. Klymchenko, Liquid ordered and gel phases of lipid bilayers: fluorescent probes reveal close fluidity but different hydration, Biophys. J. 95 (3) (2008) 1217–1225.
[25] H. An, M.R. Nussio, M.G. Huson, N.H. Voelcker, J.G. Shapter, Material properties of lipid microdomains: force-volume imaging study of the effect of cholesterol on lipid microdomain rigidity, Biophys. J. 99 (3) (2010) 834–844.
[26] N. Kahya, D. Scherfeld, K. Bacia, B. Poolman, P. Schwille, Probing lipid mobility of raft-exhibiting model membranes by fluorescence correlation spectroscopy, J. Biol. Chem. 278 (30) (2003) 28109–28115.
[27] A. Filippov, G. Oradd, G. Lindblom, Domain formation in model membranes studied by pulsed-field gradient-NMR: the role of lipid polyunsaturation, Biophys. J. 93 (9) (2007) 3182–3190.
[28] P.F.F. Almeida, W.L.C. Vaz, T.E. Thompson, Percolation and diffusion in 3-component lipid bilayers — effect of cholesterol on an equimolar mixture of 2 phosphatidylcholines, Biophys. J. 64 (2) (1993) 399–412.
[29] R.F. de Almeida, A. Fedorov, M. Prieto, Sphingomyelin/phosphatidylcholine/cholesterol phase diagram: boundaries and composition of lipid rafts, Biophys. J. 85 (4) (2003) 2406–2416.
[30] M. Gandhavadi, D. Allende, A. Vidal, S.A. Simon, T.J. McIntosh, Structure, composition, and peptide binding properties of detergent soluble bilayers and detergent resistant rafts, Biophys. J. 82 (3) (2002) 1469–1482.
[31] H.A. Rinia, M.M. Snel, J.P. van der Eerden, B. de Kruijff, Visualizing detergent resistant domains in model membranes with atomic force microscopy, FEBS Lett. 501 (1) (2001) 92–96.
[32] H.X. Liao, et al., A group M consensus envelope glycoprotein induces antibodies that neutralize subsets of subtype B and CHIV-1 primary viruses, Virology 353 (2) (2006) 268–282.
[33] R.M. Scearce, G.S. Eisenbarth, Production of monoclonal antibodies reacting with the cytoplasm and surface of differentiated cells, Methods Enzymol. 103 (1983) 459–469.
[34] R.C. MacDonald, et al., Small-volume extrusion apparatus for preparation of large, unilamellar vesicles, Biochim. Biophys. Acta 1061 (2) (1991) 297–303.